2024 IEEE 63rd Conference on Decision and Control (CDC)
December 16-19, 2024. MiCo, Milan, Italy

State Boundary Avoidance Control of Dielectric Elastomer Actuator for Material Safety Assurance

Theophilus Kaaya, Zheng Chen*

Abstract— **Dielectric Elastomer Actuators (DEAs) have been used in various applications in wearable assistive devices and energy harvesting systems. However, material safety assurance control, which prevents dielectric elastomer failures, is not fully investigated. In this work, a state boundary avoidance control of DEA for material safety assurance is developed. Since various DEA configurations share common failure modes, incorporating these modes into the system is crucial for extending DEA lifetime and improving robustness. To expand the DEA's working range, the algorithm for internal safety control allows operation within a broader feasible region while preventing electrical breakdown (EB), electromechanical instability (EMI), loss of tension (LT), or rupture by stretch (RS). This algorithm prioritizes safety control when the feasible space is violated and allows primary control when operating within the safe space. Two case studies to validate the theory are discussed for reference tracking and energy harvesting. An algorithm for internal safety control in DEAs, considering both closed and open-loop control for reference tracking and energy harvesting, is proposed. The safety control algorithm can maximize energy harvesting output power without violating material safety rules, making it applicable to various energy source conversions like human motion, tidal wave, and wind energy.**

Keywords- Dielectric Elastomer Actuator, Safety Control

I. Introduction

Dielectric elastomers are the elastomers that are coated with compliant electrodes. Applying electric voltage across the elastomer will cause contraction in thickness direction [1]. Dielectric elastomer (DE) has similar energy density with human skeletal muscles in term of output energy per volume or mass [2], which won its nickname "artificial muscle". Safety control of Dielectric Elastomer Actuators (DEAs) comes in many forms depending on the objective and use of the DEA. The most common concern of DEA safety control is with human interaction. Since DEAs are known to be operated at high voltages, there is a need of electrical safety of the DEAs in applications that involve human interactions [3]. Other safety measures that have been employed include use of passive membranes [4], and protective measures such as sand witching the live electrode with the grounded electrode [5] to mention but a few.

However, it is known that the DEAs do fail in multiple modes when their internal thermodynamic state reaches critical values [6], [7]. It is not common to find literature that addresses the safety control of DEAs within these fail safe modes. In this paper, we propose a control algorithm that offers internal safety of the DEA while it is operated in closed and open loop control for reference tracking and energy harvesting [8]. Different configurations of DEAs exist such as stacked, diaphragm (a kind of planar DEAs), rolled, and tubular [9]–[11]. All these configurations are governed by the same failure modes. Incorporating these modes into the DEA system will prolong the lifetime of the DEA and improve the DEA robustness. In particular, the planner DEA configurations are employed in applications such as micropumps chips [12], grippers, swimming robots, wearable devices, and elastomeric lenses [13] For control applications, various control schemes have been proposed and employed such as H_∞ controller to handle model uncertainty, disturbance rejection, and sensor noise [11], [14]. Sliding mode control for hysteresis management and handing complex nonlinearities of the DEA [15], [16]. PID control and its adaptations for practical implementation and ease of control [17]–[19]. In our recent work [10], adaptive iterative learning control is implemented on a roll actuator for active compression applications in the lower limbs.

All these control applications however do not put into consideration the thermodynamic state of the DEAs and so are operated in a limited regime to ensure their functionality. To increase the working region of the DEAs, internal safety control mechanism must be employed allowing the actuator to move from one state to another within the feasible region. Access to a wider space of operation allows for maximum output from the DEAs, increased performance, durability, and lifespan. With internal safety implemented, electrical safety can also be embedded in the safety control algorithm for added functionality and robustness. A major contribution of this paper is the development of an algorithm for internal safety control developed for both reference tracking allowing the DEA to be operated in a wider range of space while preventing the DEA from breaking via the failure modes mentioned above. When used for energy harvesting with the safety control measures in place, the DEA is able to provide larger power output as previously reported for a given cycle of power generation [7]. The algorithm, used as a safety control measure in line with the primary control, prioritizes safety when the feasible space is violated and allows for primary control when the operation is within the safe space. This allows for increased energy transferring from mechanical loading to electrical output. The energy harvesting can be executed while an individual walks, or from tidal wave energy, or wind energy.

The rest of the paper is arranged as follows: Section II

*Corresponding author: Zheng Chen, Email: zchen43@central.uh.edu.
This work is supported in part by the National Science Foundation under Grant CMMI #1747855.
T. Kaaya and Z. Chen are with the University of Houston, Mech. Eng. Dept, 4800 Calhoun Rd, Houston TX 77004. tskaaya@uh.edu, zchen43@central.uh.edu

discusses the dynamic modeling of the DEA accounting for viscous effects and strain hardening. Section III discusses the modes of failure of the DEA and provides an algorithm that can be used as a safety control measure. Section IV introduces the control schemes designed for the DEA, Section V discusses the simulation case studies for reference tracking and energy harvesting, and finally, Section VI discusses the conclusion and future work.

II. Modeling of the DEA

Fig. 1 shows a schematic of the dielectric membrane subject to in-plane bi-axial force loading and voltage application through the thickness using compliant electrodes. In the undeformed state, the DEA has a length and width

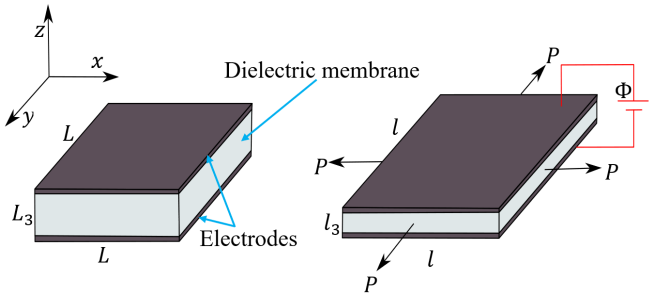

Fig. 1. DEA schematic

of L and a thickness of L_3. When a mechanical force, P or voltage load, Φ is applied, the DEA deforms to a new length and width l and thickness l_3. The DEA is modeled as an ideal planar dielectric elastomer with viscous stiffening. The viscoelastic model is made up of two parallel elements, a spring in one element and a spring and dash-pot in another element. A Gent model of the DEA is used to account for strain stiffening. The DEA model is adopted from [20]. The governing equation of motion of the DEA is

$$\frac{\rho L^2}{3\mu}\frac{d^2\lambda}{dt^2}+\frac{\chi(\lambda-\lambda^{-5})}{1-(2\lambda^2+\lambda^{-4}-3)/J^A}+\frac{1}{2}\frac{c}{\mu L_3}\frac{d\lambda}{dt} +\frac{(1-\chi)(\lambda\zeta^{-2}-\lambda^{-5}\zeta^4)}{1-(2\lambda^2\zeta^{-2}+\lambda^4\zeta^4-3)/J^B}-\frac{\varepsilon}{\mu}\left(\frac{\Phi}{L_3}\right)^2\lambda^3-s=0 \tag{1}$$

where ρ is the density of the dielectric membrane, $\mu=\mu^A+\mu^B$ is the shear modulus of the DEA, μ^A and μ^B are the shear moduli of the two springs, λ is the elastic (spring) membrane stretch, $\chi=\mu^A/\mu$ is the ratio between the equilibrium and instantaneous moduli, J^A and J^B are the extension limits, ζ is the dissipative (dash-pot) membrane stretch, ε is the elastomer permittivity, Φ is the voltage on the membrane, $s=P/(LL_3)$ is the nominal stress where P is the mechanical force, and c is the damping coefficient. The rate of stretch in the dash-pot is

$$\frac{d\zeta}{dt}=\frac{\zeta\mu^B}{6\eta}\frac{(\lambda^2\zeta^{-2}-\lambda^{-4}\zeta^4)}{1-(2\lambda^2\zeta^{-2}+\lambda^{-4}\zeta^4-3)/J^B}, \tag{2}$$

where η is the dash-pot viscosity. The DEA is also treated as an RC series circuit with the membrane voltage dynamics as

$$\dot{\Phi}=-\left(\frac{\dot{C}}{C}+\frac{1}{RC}\right)\Phi+\frac{u}{RC}, \tag{3}$$

where R is the resistance of the DEA, C is the membrane capacitance, and u is the applied voltage to the DEA. Assuming the DEA as a parallel plate capacitor, the capacitance can be expressed as

$$C=\varepsilon\frac{A}{L_3}=\frac{\varepsilon L^2}{L_3}\lambda^4. \tag{4}$$

Eq. (1) to (4) are used to form the fully coupled state space equation of the DEA with the states $x=[x_1,x_2,x_3,x_4,x_5]=[\lambda,\dot{\lambda},\zeta,\Phi,C]$. The state space equation is

$$\begin{aligned}
\dot{x_1}&=x_2,\\
\dot{x_2}&=\frac{3\mu}{\rho L^2}\left[-\frac{\chi(x_1-x_1^{-5})}{1-(2x_1^2+x_1^{-4}-3)/J^A}-\frac{1}{2}\frac{c}{\mu L_3}x_2\right.\\
&\quad\left.-\frac{(1-\chi)(x_1x_3^{-2}-x_1^{-5}x_3^{-4})}{1-(2x_1^2x_3^{-2}+x_1^4x_3^4-3)/J^B}+\frac{\varepsilon}{\mu}\left(\frac{x_4}{L_3}\right)^2x_1^3+s\right],\\
\dot{x_3}&=\frac{x_3\mu^B}{6\eta}\frac{(x_1^2x_3^{-2}-x_1^{-4}x_3^{-4})}{1-(2x_1^2x_3^{-2}+x_1^{-4}x_3^4-3)/J^B},\\
\dot{x_4}&=-\left[\frac{1}{x_5}\frac{4\varepsilon L^2}{L_3}x_1^3x_2+\frac{1}{Rx_5}\right]x_4+\frac{u}{Rx_5},\\
\dot{x_5}&=\frac{4\varepsilon L^2}{L_3}x_1^3x_2,
\end{aligned} \tag{5}$$

where s and u are the inputs to the system. With the state space equation defined, the modes of failure can be evaluated provided the equation of state of the DEA as described in Section III.

III. Modes of Failure and Safety Control Algorithm of the DEA

DEAs may fail in various modes such as, mechanical rupture, electrical breakdown, electromechanical instability, and loss of tension [6], [7]. Given the equation of state of the DEA as [7]

$$\frac{s}{\mu}=\lambda-\lambda^{-5}-\left(\frac{\bar{D}^2}{\varepsilon\mu}\right)\lambda^{-5}, \tag{6}$$

$$\frac{\bar{E}}{\sqrt{\mu/\varepsilon}}=\left(\frac{\bar{D}}{\sqrt{\varepsilon\mu}}\right)\lambda^{-4}, \tag{7}$$

where $\bar{E}=\Phi/L_3$ is the nominal electric field, $\bar{D}=Q/L^2$ is the nominal electric displacement, and Q is the charge on the membrane. When the membrane is uncharged, $\bar{D}=\bar{E}=0$, Eq. (6) becomes

$$\frac{s}{\mu}=\lambda-\lambda^{-5}, \tag{8}$$

setting the upper bound on the nominal stress of the DEA.

The DEA may fail by electrical breakdown (EB) when a critical electric field, E_{EB} is reached. This sets the EB criteria

as

$$\frac{s}{\mu} = \lambda - \lambda^{-5} - \left(\frac{E_{EB}^2}{\mu/\varepsilon}\right)\lambda^{-1}, \tag{9}$$

$$\frac{\bar{E}}{\sqrt{\mu/\varepsilon}} = \left(\frac{E_{EB}^2}{\mu/\varepsilon}\right)\left(\frac{\bar{D}}{\sqrt{\varepsilon\mu}}\right)^{-1}. \tag{10}$$

The DEA may also fail due to electromechanical instability (EMI) as the membrane thickness reduces [7]. This happens when

$$\frac{s}{\mu} = \frac{2}{3}(\lambda - 4\lambda^{-5}), \tag{11}$$

$$\frac{\bar{E}}{\sqrt{\mu/\varepsilon}} = \left(\frac{\bar{D}}{\sqrt{\varepsilon\mu}}\right)\left(3\frac{\bar{D}^2}{\varepsilon\mu} - 5\right)^{-2/3}. \tag{12}$$

Additionally, the membrane may fail due to loss of tension, $s = 0$. This implies that

$$\frac{\bar{E}}{\sqrt{\mu/\varepsilon}} = \left(\frac{\bar{D}}{\sqrt{\varepsilon\mu}}\right)\left(1 + \frac{\bar{D}^2}{\varepsilon\mu}\right)^{-2/3}. \tag{13}$$

Lastly, the DEA may fail due to rupture by stretch when the stretch reaches a critical value, λ_R. This gives

$$\frac{\bar{E}}{\sqrt{\mu/\varepsilon}} = \left(\frac{\bar{D}}{\sqrt{\varepsilon\mu}}\right)\lambda_R^{-4} \tag{14}$$

Fig. 2 shows the thermodynamic state of the DEA in the force-displacement plane and the voltage-charge plane. The gray region is the safe/feasible region that the DEA is required to operate. To ensure that the DEA remains in the feasible region, a safety control algorithm is proposed as shown in the Pseudo Algorithm 1.

Algorithm 1 Safety Control Algorithm

```
Check constraints
if Any of the constraints are violated then ▷ (short-circuit OR)
    if Loss of tension violated then
        s_safe = Tensionloss_bias
        u_safe = 0
    else if No charge violated then
        s_safe = NoCharge_constraint + NoCharge_bias
        u_safe = 0
    else if EMI violated then
        s_safe = EMI_constraint + EMI_bias
        u_safe = 0
    else if EB violated then
        s_safe = EB_constaint + EB_bias
        u_safe = 0
    else if Rapture violated then
        s_safe = s_safe(t − 1)
        u_safe = 0
    else ▷ None of the above conditions are met
    end if
else ▷ All constraints satisfied, use applied values
end if
```

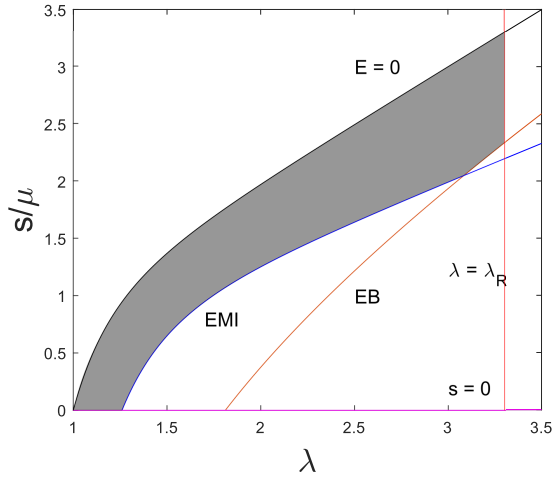

(a)

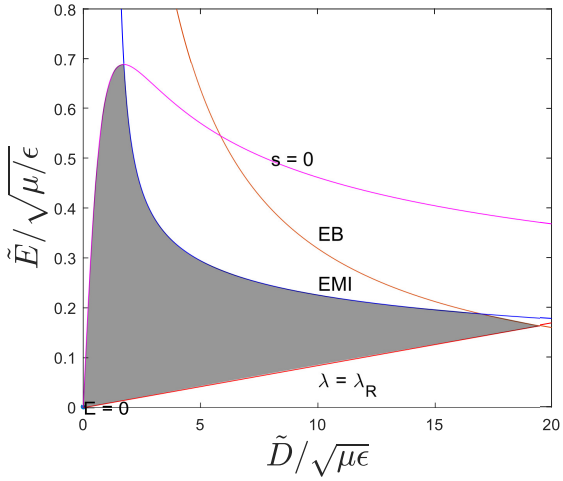

(b)

Fig. 2. Safe/feasible thermodynamic state of the DEA in the a) force-displacement plane and b) voltage-charge plane

To determine which mode of failure is violated, the equation of state, Eq. (6) and Eq. (7), needs to be known. The stress, s can be determined from a force sensor attached to the rack and pinion gear system. λ can be determined through self-sensing of the DEG using the measured capacitance, Eq. (4). $\bar{E}$ is determined from the voltage on the membrane and the unstretched membrane thickness, and $\bar{D} = Q/L^2 = (C\Phi)/L^2$ determined from the capacitance and voltage across the DE membrane. The algorithm assumes a quasi-static DEA state making it mostly effective with slow actuation. For very fast actuation, the dynamics of state need to be considered to have a more effective safety controller. This is to be explored in our future work having demonstrated that the safety controller can work in a quasi-static setting. Having established the DEA state, the algorithm is able to determine which side of the boundary constraints the DEA lies, safe (gray) or unsafe region (white). Since the algorithm uses the static state of the DEG, bias terms and safety factors are included in the safety check and safe control to ensure that the DEG does not cross the true safety boundaries

as might be observed later on in Fig. 6. the algorithm is designed to first remove any applied voltage, this is intended to move the actuator away from the EMI and EB boundary quickly moving it towards the stretch limit or loss of tension boundaries that are mechanical in nature and easily dealt with. It should be noted that the algorithm boundaries are placed inside the true boundaries providing a buffer from which a corrective measure can be employed before the DEA can reach the true failure modes. This buffer is what allows the algorithm to function ahead of the actuator truly crossing the true boundaries hence ensuring the goodness of the actuator and keeping it within the safety region. The flow of the algorithm is as follows: First, the algorithm checks for any violation of the failure modes. If any of the modes is violated, it proceeds to determine which mode in particular is violated, thereby correcting the violation to keep the DEA within the feasible region. The safe control is determined as one that will drive the DEA along the boundary of the failure mode ($*_{constraint}$) plus an added bias ($*_{bias}$) to keep the DEA well within the feasible space. Otherwise, if no failure mode is violated, the safety control algorithm allows the primary control to go through. It is assumed that the stress s applied to the DEA can be controlled via force feedback while the voltage u is controlled via on and off switching.

IV. Control Design for DEA reference tracking

In this section, the control scheme for reference tracking of the DEA stretch, λ with the safety control algorithm is proposed. Two primary control methods are explored, a Sliding Mode Control (SMC) and Proportional-Integral-Derivative (PID) control. Considering Eq. (5), there are two ways of controlling the DEA. One is through application of the mechanical force via the stress, s. Another is through application of a voltage, u to induce a voltage, Φ across the membrane of the DEA. So the system is a multiple input single output (MISO) system as shown in Fig. 3. C_1 and C_2 are the controllers that control s and u. For control

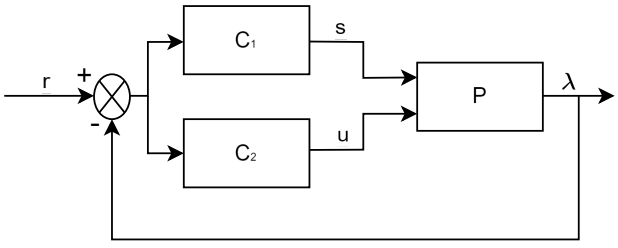

Fig. 3. Block Diagram For Reference Tracking Control

purposes, two control schemes are employed. The first uses SMC in combination with PID control for the two control channels s and u respectively while the second uses only PID controls on the two control channels. The schemes are used to archive reference tracking for the DEA while keeping the DEA constrained within the safe region via the Safety Control Algorithm.

A. Sliding Mode Control

The DEA system is a highly nonlinear system. For reference tracking, error dynamics are introduced to setup the sliding surface for the SMC. The error, e in tracking a stretch reference, r is $e = r - x_1$. Since the mechanical force and induced voltage show up in the stretch rate of the DEA, the error dynamics are evaluated up to the second derivative:

$$\begin{aligned} \dot{e}_1 &= e_2, \\ \dot{e}_2 &= \ddot{r} - f_2 - bx_4^2 - ds, \end{aligned} \tag{15}$$

where $e_1 = e$, $e_2 = \dot{e}$, and the terms, f_2, b, and d are

$$\begin{aligned} f_2 = \frac{3\mu}{\rho L^2}\Bigg[&-\frac{\chi(x_1 - x_1^{-5})}{1-(2x_1^2 + x_1^{-4} - 3)/J^A} \\ &-\frac{(1-\chi)(x_1 x_3^{-2} - x_1^{-5} x_3^{-4})}{1-(2x_1^2 x_3^{-2} + x_1^4 x_3^4 - 3)/J^B} - \frac{1}{2}\frac{c}{\mu L_3} x_2\Bigg], \\ b = \frac{3\varepsilon}{\rho L^2 L_3^2} x_1^3, \quad d = &\frac{3\mu}{.}\rho L^2 \end{aligned} \tag{16}$$

Let the sliding surface, $\mathfrak{S}$ be

$$\mathfrak{S} = c_1 e_1 + c_2 e_2, \tag{17}$$

where $c_1 > 0$ and $c_2 > 0$ are constants that control the rate of convergence of the sliding surface. The objective is to design s and u such that the error dynamics are asymptotically stable. In this case, the control s is designed for SMC while u is set as PID control. s is designed such that

$$\dot{\mathfrak{S}} = c_1 \dot{e}_1 + c_2 \dot{e}_2 = -k\,\mathrm{sgn}(\mathfrak{S}), \tag{18}$$

where k defines the rate of convergence of the sliding surface. Substituting for $\dot{e}_1$ and $\dot{e}_2$, and solving for s produces the control law

$$s = \frac{1}{d}\left[\frac{c_1}{c_2}(\dot{r} - x_2) + (\ddot{r} - f_2 - bx_4^2) + \frac{k}{c_2}\,\mathrm{sgn}(\mathfrak{S})\right] \tag{19}$$

It is worth noting that SMC requires the reference to be continuously differentiable or piece wise differentiable for smooth control. This should be taken into account when setting up a reference tracking problem that will violate rupture by stretch when $\lambda = \lambda_R$.

B. Proportional-Integral-Derivative Control

The PID control, $G_c(s_1)$ used for the DEA is of the form

$$G_c(s_1) = P + \frac{I}{s_1} + D\frac{N}{1 + \frac{N}{s_1}}, \tag{20}$$

where P is the proportional gain, I is the integral gain, D is the derivative gain, N is the filter coefficient for the first-order pole filter of the derivative action, and s_1 is the Laplace variable [21].

V. Simulation of Two Case studies

In the simulation case study, the safety control algorithm is used in reference tracking and open loop control for energy harvesting from the DEA acting as a generator. With the implementation of safety control algorithm, the DEA can be controlled to prioritize and maintain safety when a given reference violates the allowable stable state of the DEA. Likewise, the area enclosed by the cycle of the DEA generator can be increased to provide a larger energy of conversion from the one in [7]. The parameters for simulation are shown in Table I.

TABLE I

PARAMETERS FOR SIMULATION

Parameter	Value	Unit
Thickness (L_3)	1	mm
Length (L)	6	mm
m	5	g
ε_r	2.7	
c	0.5	Ns/m
R	1	GΩ
μ	1	MPa
η	1.78	MPa· s
$J^A = J^B$	350	
c_1, c_2, k	3, 1, 500	
$(P,I,D,N)_s$	(5.5, 0.9, 0.01, 500)	
$(P,I,D,N)_u$	(1, 0.1, 0.1, 2000)	

A. Reference Tracking

To demonstrate the ability of the safety control algorithm, the simulation is setup to start with the DEA in an unstretched state, $\lambda = 1$ thus placing the DEA at the boundary of loss of tension, $s = 0$. Fig. 4 shows the results of a sinusoidal reference tracking signal where both s and u are controlled using PID only vs, a combination of PID control on u and SMC on s. It can be observed that both PID only control and PID combined with SMC control can track the reference signal and keep the safe reference when $\lambda > \lambda_R$. In terms of performance, including SMC provides better tracking compared to PID only. This is because the SMC can deal with the non linearity of the system while PID only is susceptible to instability when the controllers are set to be aggressive.

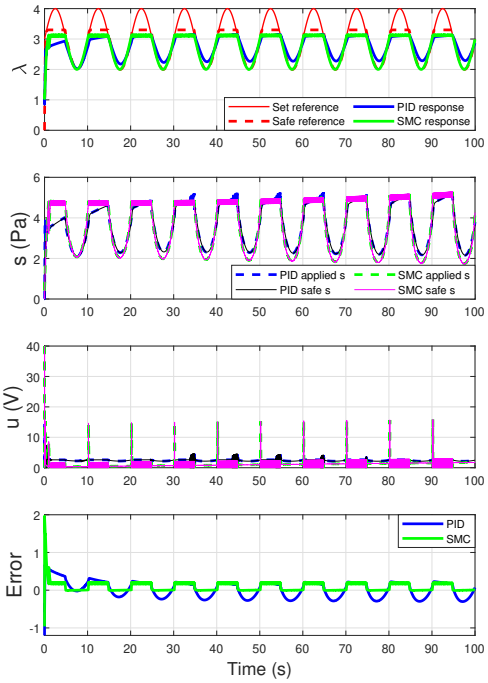

Fig. 4. Reference Tracking Response with Safety Control

The thermodynamic state of the DEA is shown in Fig. 5 during reference tracking in the force-displacement plane and voltage-charge plane. Since most of the stretch is by mechanical strain, the voltage component does not produce a large enough voltage to affect the system significantly. In the voltage-charge plane, Fig. V-A, it is observed that the DEA remains inside the allowable bounds of loss of tension and rupture by stretch.

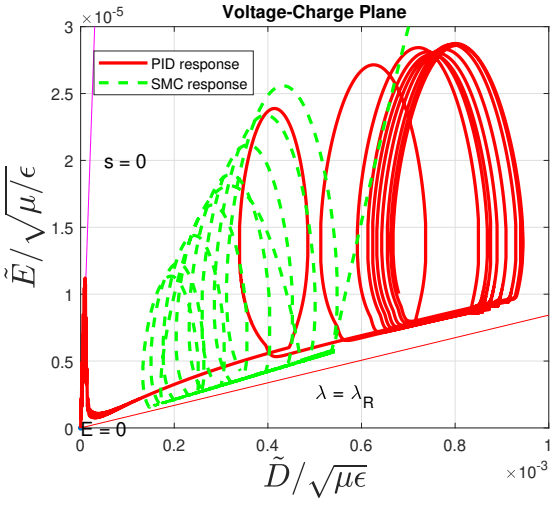

Fig. 5. Reference Tracking Thermodynamic State with Safety Control

B. Energy Harvesting

This section discusses the increase in energy conversion of the DEA while maintaining safety when the DEA is used as a generator [7]. A constant voltage u is applied on the DEA and a cyclic loading applied on s. Through mechanical loading of the DEA, the mechanical energy provided to the DEA can be converted to electricity with the safety control algorithm allowing the DEA to operate within the feasible region. Provided a cyclic loading s, the safety control algorithm can be used to drive the DEA such that it remains within the feasible range covering a larger area of the feasible space. By following the feasible space boundaries, there is room for increasing the energy conversion from mechanical loading to electrical energy. Fig. 6 shows the thermodynamic state trajectory under a cyclic loading of amplitude 3 Pa. Since most commom applications of DEAs require a pre-stretch, the safety controller is designed such that there is a minimum predefined stretch for the membrane. The simulation is set up to start running from an unstretched state of the DEA to demonstrate that the safety controller can move the DEA from the loss of tension state and keep it actuated at or above the desired minimum pre-stretched as is observed at the first cycle of the simulation. The algorithm is able to choose a safe mechanical loading on the DEA allowing it to operate at extreme regions for a longer time hence increasing the energy output. Fig. 6 also shows the energy conversion of the DEA in open loop mode with a constant voltage applied to the DEA.

The area, enclosed by the DEA response represents the total energy that can be converted and utilised for electricity without limiting the cycles to those based on the dashed line

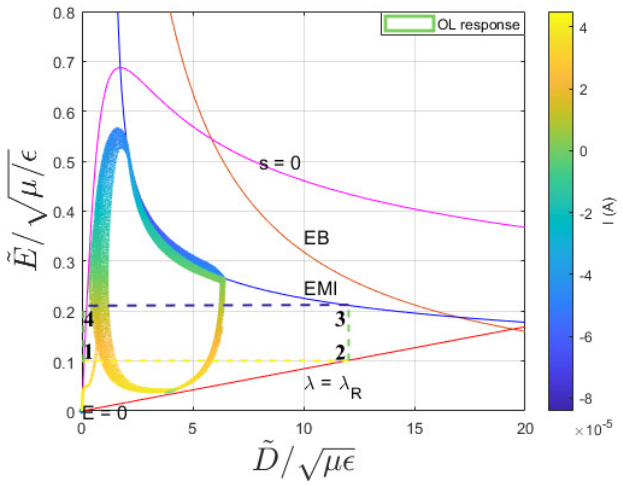

Fig. 6. Thermodynamic state under 3 Pa cycling loading

as shown in Fig. V-B. The four-cycle scheme requires two batteries. One supplies charge at a low voltage Φ_{in}, and the other stores charge at a high voltage Φ_{out}. From state 1 to state 2, the elastomer is switched to the input battery and is pulled from a small stretch up to the stretch of rupture. From state 2 to state 3, the elastomer is switched to an open circuit, and the tensile force is reduced, allowing the elastomer to thicken until it is close to EMI. From state 3 to state 4, the elastomer is switched to the output battery, and the tensile force is further reduced until the condition of loss of tension. From state 4 back to state 1, the elastomer is once again switched to an open circuit, and the tensile force is increased, allowing the elastomer to reduce the thickness.

With the safety control scheme, the DEA is able to travel along the EMI boundary allowing more charge to be transferred to the output battery source. As such the power output is increased as shown in Fig. V-B. The conversion of mechanical energy to electrical energy using the DEA can find its application activities that have cyclic mechanic loading such as walking where appliances can be charged. It could be used to harvest tidal wave energy and wind energy.

VI. Conclusion and Future Work

In this work, reference tracking of the DEA using PID and SMC with an enforced safety control algorithm is proposed with simulations results showing safety enforcement. Since SMC is a nonlinear controller it offers better performance than the PID when observing safety. This is a trade off that the PID does not provide as it compromises performance in favour of safety. Likewise, the DEA can be used for energy harvesting as a generator converting mechanical energy into electrical energy. With the implementation of the safety algorithm, more energy from mechanical cyclic loading can be harvested without breaking the DEA. Given the simulation results, future work will include applying the safety control algorithm on a physical DEA to compare results with the experimental data. The safety control algorithm could also be simplified and optimized to increase its applicability in real world scenarios. In addition, a second-order sliding mode control (SOSMC) can be employed to reduce the chattering experienced when switching from primary to safe control.

References

[1] Y. Bar-Cohen, "Electroactive polymers: current capabilities and challenges," in *Smart Structures and Materials 2002: Electroactive Polymer Actuators and Devices (EAPAD)*, vol. 4695. SPIE, 2002, pp. 1–7.

[2] R. Pelrine, R. Kornbluh, J. Joseph, R. Heydt, Q. Pei, and S. Chiba, "High-field deformation of elastomeric dielectrics for actuators," *Materials Science and Engineering: C*, vol. 11, no. 2, pp. 89–100, 2000.

[3] S. Pourazadi, A. Shagerdmootaab, H. Chan, M. Moallem, and C. Menon, "On the electrical safety of dielectric elastomer actuators in proximity to the human body," *Smart Materials and Structures*, vol. 26, no. 11, p. 115007, oct 2017.

[4] G. Frediani, D. Mazzei, D. E. De Rossi, and F. Carpi, "Wearable wireless tactile display for virtual interactions with soft bodies," *Front Bioeng Biotechnol*, vol. 2, p. 31, Sep. 2014.

[5] J. Shintake, D. Ichige, R. Kanno, T. Nagai, and K. Shimizu, "Monolithic stacked dielectric elastomer actuators," *Frontiers in Robotics and AI*, vol. 8, 2021.

[6] Z. Suo, "Theory of dielectric elastomers," *Acta Mechanica Solida Sinica*, vol. 23, no. 6, pp. 549–578, 2010.

[7] S. J. A. Koh, X. Zhao, and Z. Suo, "Maximal energy that can be converted by a dielectric elastomer generator," *Applied Physics Letters*, vol. 94, no. 26, p. 262902, 06 2009.

[8] G. Thomson, D. Yurchenko, and D. V. Val, "Dielectric elastomers for energy harvesting," in *Energy Harvesting*, R. Manyala, Ed. Rijeka: IntechOpen, 2018, ch. 4.

[9] G. Kovacs, L. Düring, S. Michel, and G. Terrasi, "Stacked dielectric elastomer actuator for tensile force transmission," *Sensors and actuators A: Physical*, vol. 155, no. 2, pp. 299–307, 2009.

[10] T. Kaaya, R. J. Venkatraman, D. Koc, and Z. Chen, "Modeling and control of dielectric elastomer enabled cuff device for enhancing blood flow at lower limbs," *IEEE Transactions on Automation Science and Engineering*, pp. 1–10, 2023.

[11] T. Kaaya, S. Wang, M. Cescon, and Z. Chen, "Physics-lumped parameter based control oriented model of dielectric tubular actuator," *International Journal of Intelligent Robotics and Applications*, vol. 6, no. 3, pp. 397–413, Sep. 2022.

[12] X. Pang, B. Li, D. Xia, and S. Jing, "Application of dielectric elastomer planar actuators in a micropump chip," in *2009 4th IEEE Conference on Industrial Electronics and Applications*, 2009, pp. 1199–1202.

[13] J.-H. Youn, S. M. Jeong, G. Hwang, H. Kim, K. Hyeon, J. Park, and K.-U. Kyung, "Dielectric elastomer actuator for soft robotics applications and challenges," *Applied Sciences*, vol. 10, no. 2, 2020.

[14] Z. Ye, Z. Chen, R. Asmatulu, and H. Chan, "Robust control of dielectric elastomer diaphragm actuator for human pulse signal tracking," *Smart Materials and Structures*, vol. 26, no. 8, p. 085043, jul 2017.

[15] J. MacLean, J. Zou, G. Gu, V. Vaziri, and S. S. Aphale, "Sliding-mode control of a dielectric elastomer actuator featuring non-invertible dynamics," in *2021 27th International Conference on Mechatronics and Machine Vision in Practice (M2VIP)*, 2021, pp. 1–6.

[16] J. Zou, J. D. J. MacLean, J. Ren, S. S. Aphale, and G. Gu, "Proxy-based sliding-mode tracking control of dielectric elastomer actuators through eliminating rate-dependent viscoelasticity," *Smart Materials and Structures*, vol. 31, no. 10, p. 104002, sep 2022.

[17] T. Karner and J. Gotlih, "Position control of the dielectric elastomer actuator based on fractional derivatives in modelling and control," *Actuators*, vol. 10, no. 1, 2021.

[18] C.-Y. S. Peng Huang, Jundong Wu and Y. Wang, "Tracking control of soft dielectric elastomer actuator based on nonlinear pid controller," *International Journal of Control*, vol. 97, no. 1, pp. 130–140, 2024.

[19] Z. Xing and H. Yong, "Nonlinear dynamic behaviors and pid control of viscoelastic dielectric elastomer balloons," *Journal of Intelligent Material Systems and Structures*, vol. 33, no. 11, pp. 1449–1464, 2022.

[20] J. Sheng and Y. Zhang, "Dynamic electromechanical response of a viscoelastic dielectric elastomer under cycle electric loads," *International Journal of Polymer Science*, vol. 2018, p. 2803631, Jan 2018.

[21] S. Documentation, "Pid controller," 2023.